Nanoscale

Accepted Manuscript

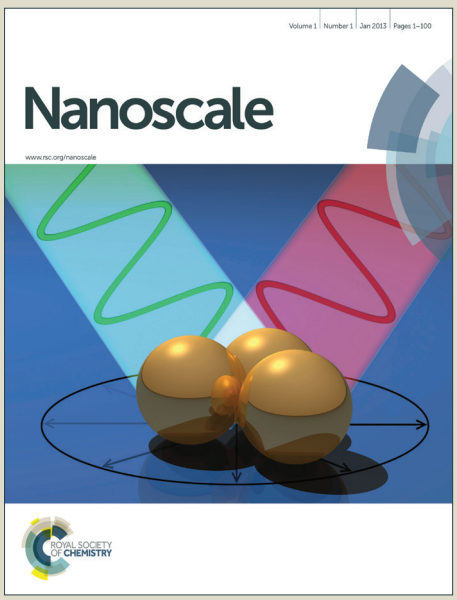

ROYAL SOCIETY OF CHEMISTRY

www.rsc.org/nanoscale

Cite this: DOI: 10.1039/c0xx00000x

www.rsc.org/xxxxxx

ARTICLE TYPE

Hierarchical $MnCo_2O_4$ nanosheets arrays/carbon cloth as integrated anodes for lithium-ion full batteries with improved performance

Xiaojuan Hou,[a] Xianfu Wang,[a,b] Bin Liu,[a,b] Qiufan Wang,[a] Tao Luo,[a,b] Di Chen*,[a] and Guozhen Shen*,[a,b]

Received (in XXX, XXX) Xth XXXXXXXXX 20XX, Accepted Xth XXXXXXXXX 20XX

DOI: 10.1039/b000000x

To solve the reduced output voltage caused by the high lithium redox potential of Co_3O_4 when applied as anode material in full cells, an effective strategy to partially replace Co by Mn to form $MnCo_2O_4$ without changing the original crystal structure. Herein, 3D hierarchical $MnCo_2O_4$ nanosheets arrays grown via a hydrothermal method on carbon cloths, as binder-free anodes for lithium-ion batteries, exhibit a high areal capacity of 3.0 mAh cm^{-2} at a current density of 800 μA cm^{-2}, excellent cycling stability, good rate performances and relatively proper discharge voltage plateau with 0.25 V lower than the Co_3O_4 nanosheets counterparts. Due to the increased output voltage of the full cell induced by the introduction of Mn species with a lower lithium extraction potential, $MnCo_2O_4$ based full cells display relatively higher or comparative capacity in a certain voltage range compared with the Co_3O_4, while still keeps the excellent conductivity of Co_3O_4 electrodes. Our work here paves a way for design of high performance full cells with Co-based oxides electrodes.

Introduction

In recent years great efforts have been advocated to design rechargeable lithium-ion batteries due to their advantages such as high energy density, long lifespan and environmental benignity widely applied as power sources for portable electronic devices.[1-5] A major research direction is the exploitation of anode materials with high reversible capacity, rate performance and long cycle life.[6-9] Amongst the available materials, Co_3O_4 has received much attention since its high theoretical capacity of 890 mAh g^{-1}.[10-13] However, its high lithium redox potential would generate high average voltage, thus leading to the reduced output voltage when applied as anode material in full cells, which may perform poor performances at the relatively high potential when tested in a certain potential range. Meanwhile, the high cost of cobalt element also makes it not an ideal anode material in practical applications. Since manganese (Mn) is 20 times less expensive than cobalt, more abundant in nature and especially manganese-based oxides possess lower operating voltage for lithium-ion batteries,[14-16] the introduction of Mn species into cobalt-based oxides electrodes may be an effective strategy to improve the performance of lithium-ion batteries, while still keeps the excellent conductivity of cobalt-based oxides.[17]

Recently, lots of researches have confirmed that complex oxides containing two or more kinds of metal ions show good electrochemical performances because of their synergetic effects during the charge/discharge process.[18-24] Therefore considering the advantages and disadvantages of both Co-based and Mn-based electrodes materials, as well as $MnCo_2O_4$ possessing better performances than $CoMn_2O_4$ under the same condition according to the previous reports,[17,20] we choose the $MnCo_2O_4$ as the anode material adopting the excellent half cells performances of Co_3O_4 and high output voltage of Mn species. Studies have found that the electrochemical performances of $MnCo_2O_4$ such as reversible capacity, cyclic stability or rate performance are not very well.[25-30] Therefore the $MnCo_2O_4$ electrodes with excellent performances are now highly desired. In addition $MnCo_2O_4$ has the same crystal structure, approximate lattice constant and same valence states of Co and Mn with Co_3O_4, which can be regarded as the partial replacement of approximate 1/3 Co by Mn and its simple cubic structure can provide sufficient space for lithium-ion insertion.

In this paperwork, considering the superior performances of hierarchical structure in energy storage,[31-33] hierarchical $MnCo_2O_4$ nanosheets arrays were grown on textile carbon cloth considering its superior performances as substrates in energy storage[34-37] via a simple hydrothermal method. When applied as binder-free anodes, the material displayed a high capacity of 3.0 mAh cm^{-2} at a current density of 800 μA cm^{-2}, excellent cycling stability, good rate performances and relatively proper discharge voltage plateau with 0.25 V lower than their Co_3O_4 conterparts fabricated under the same conditions. The lower average voltage of $MnCo_2O_4$ electrodes leads to increased output voltage of full cells, which makes the full cells exhibited exhibit superior performances in a certain voltage range as well.

Experimental section

Material synthesis:

All of the reagents are of analytical purity and used without further purification. Before used, the commercially available textile carbon cloths were cut into desired sizes and treated with acetone, water and ethanol in sequence. In a typical process, 2 mmol $Co(CH_3COO)_2$ and 1 mmol $Mn(CH_3COO)_2$ were dissolved

in 40 ml ethylene glycol to form a clear solution, and then the mixture and a piece of carbon cloth were put into a 60 ml telflon-lined stainless steel autoclave at 200°C for 6 h. After cooled down to room temperature, the carbon cloths with deposited samples were washed several times with ethanol and dried in air at 60°C. The final products were obtained after calcinated at 400°C for 2 h in air. The Co_3O_4/carbon cloth were synthesized under the same condition except that only $Co(CH_3COO)_2$ was used instead of the mixture of $Co(CH_3COO)_2$ and $Mn(CH_3COO)_2$. The mass loading of the active material is calculated to be about 3 mg cm^{-2}.

Materials characterization:

The phase purity of the product was identified by using an X-ray diffractometer (X'Pert PRO, PANalytical B.V., The Netherlands) with radiation from a Cu target (Kα, λ=0.15406nm). The morphology was characterized by using a scanning electron microscopy (SEM, FEI Sirion 200 (10 kV). XPS measurements were performed on a VG Multilab 2000 system with a monochromatic Al Kα X-ray source.

Cell assembly and electrochemical measurements:

The electrochemical performances of the electrode were measured by assembling CR2032 coin-type half cells consisting of lithium foil as the counter electrode and reference electrode, celgard 2300 as the separator membrance, 1 M LiPF6 in a mixture of ethylene carbonate (EC) and dimethyl carbonate (DMC) (v/v = 1:1) as the electrolyte, and the as-prepared cloths directly as working electrodes without any conductive agents or polymeric binder. The coin-type full cells were fabricated with the commercial $LiCoO_2$/Al foil as the cathode, and other conditions are the same with the half cells. Cell assembly was carried out in an Ar-filled glovebox with moisture and oxygen concentrations below 1.0 ppm. Cyclic voltammogram (CV) measurements were performed on an electrochemical station (CHI 760D, CH Instruments Inc., Shanghai) at different scanning rates. The galvanostatic discharge/charge measurements were carried out on a Land Battery Measurement System (Land, China) at different current densities with a voltage window of 0.01-3.00 V for the half cells and 1.8-4.00 V for the full cells. Electrochemical impendance spectroscopy (EIS) measurements were conducted on an electrochemical workstation in a frequency range from 0.1 Hz to 100 kHz.

Results and discussion

The compositions of the as-prepared products were studied by XRD, energy dispersive spectroscopy (EDS) and XPS. Figure 1a shows the corresponding XRD pattern. All the peaks in this pattern can be indexed as face-centered-cubic (fcc) spinel $MnCo_2O_4$ (JCPDS no.1-1130) except for the peaks marked with "★", coming from the carbon cloth. In order to eliminate the influence of the carbon cloth, the powers in the same reaction system were also checked with XRD and the corresponding XRD pattern was shown in Figure S1, where all the peaks can be indexed as pure spinel $MnCo_2O_4$, further confirming the formation of pure product. EDS microanalysis of the products was shown in Figure 1b, displaying a composition of Co, Mn and O elements with Mn/Co of approximate 1/2. In order to demonstrate the detailed valence states of Mn and Co, we also carried out the XPS (Figure 1c-d) analysis. All of the binding energies were corrected for specimen charging by referring them to the C 1s peak (284.6 eV). By using a Gaussian fitting method, the Co 2p spectrum was best fitted considering two spin-orbit doubles characteristics of Co^{2+} and Co^{3+} and some shake-up satellites, while the Mn 2p spectrum features two main spin-orbit lines and little satellite structure could be observed. After refined fitting, the spectrum can be deconvolved into four peaks respectively. Figure 1c-d displays the fitting results, which can clearly present the peak position of the different valence states of Mn and Co. The results are in corresponding with the previous report about $MnCo_2O_4$.[20,30] Therefore it is reasonable that the Mn exists as Mn^{2+} and Mn^{3+}, meanwhile the Co exists as Co^{2+} and Co^{3+}. In conclusion, the solid-state redox couples of Mn^{2+}/Mn^{3+} and Co^{2+}/Co^{3+} are present in this structure, which may provide a notable electrochemical performance.

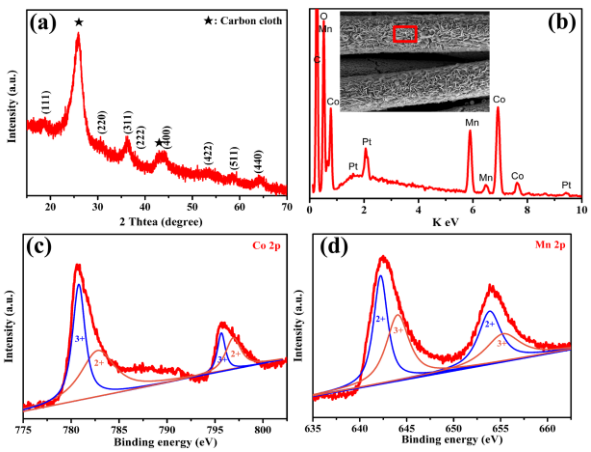

Figure 1 (a) The XRD pattern of $MnCo_2O_4$/carbon cloth. (b) The EDS microanalysis on selected areas. (c,d) XPS spectra of $MnCo_2O_4$ nanosheets.

Figure 2a-c shows the SEM images at different magnifications of the products after hydrothermal reaction, where uniform hierarchical nanosheets arrays were successfully grown on the entire carbon microfibers. Typical nanosheets are several micrometers in size and 100-200 nm in thickness. Figures 2d-f shows the SEM images of the products after calcinations of the hydrothermally grown product at 400°C for 2 h in air. From these images, we can see that the hierarchical nanosheets arrays structures of the precursors were well preserved. The thickness of the nanosheets reduced a little because of the calcination effects at high temperature.

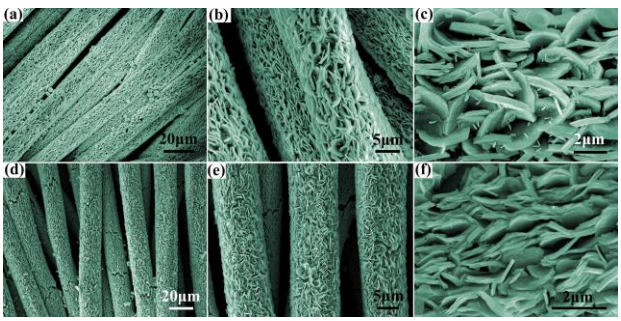

Figure 2 SEM images of the precursor (a-c) and the final nanosheets-assembled $MnCo_2O_4$/carbon cloth (d-f) at different magnifications.

To investigate the possible application of the as-grown $MnCo_2O_4$ nanostructures in lithium-ion batteries, we studied their corresponding electrochemical properties by the assembly of CR2032 coin cells by using the $MnCo_2O_4$/carbon cloth as binder-free anodes. It should be noticed that the direct growth of well assembled nanosheets arrays on carbon cloth ensures robust mechanical adhension and good electrical contact with the current collector (carbon cloth) in such addictive-free electrodes. The corresponding electrochemical performances of the $MnCo_2O_4$-based electrodes for lithium storage are shown in Figure 3. Figure 3a demonstrates the first five consecutive cyclic voltammograms (CVs) curves of the electrode at a scanning rate of 0.5 mV s^{-1} in the voltage window of 0.01-3.00 V. The first CV curve is obviously different from the following cycles and the following CV curves are almost overlapped from the second to the fifth cycles, presenting excellent reversible performances except for the irreversible reactivity in the first cycle. In the first cycle, as shown in Figure 3a, there is an obvious reduction peak around 0.5 V, which can be assigned to reduction of the metallic cation to metallic Co and Mn. In the anodic scan, two of the oxidation peaks are observed at 1.5 V and 2.0 V, corresponding to the metal to the metallic cation, while the peak around 0.4 V is ascribed to the co-efficiency between carbon cloth and the electrode material. During the following cycles, the reduction peak is removed to 0.75 V and the oxidation peaks are almost unaltered. The slight shift of the reduction peak to higher potential in the following cycles might be related to some activation process caused by the Li^+ insertion in the first cycle, meaning the slightly easier reduction in the subsequent cycles.[38,39]

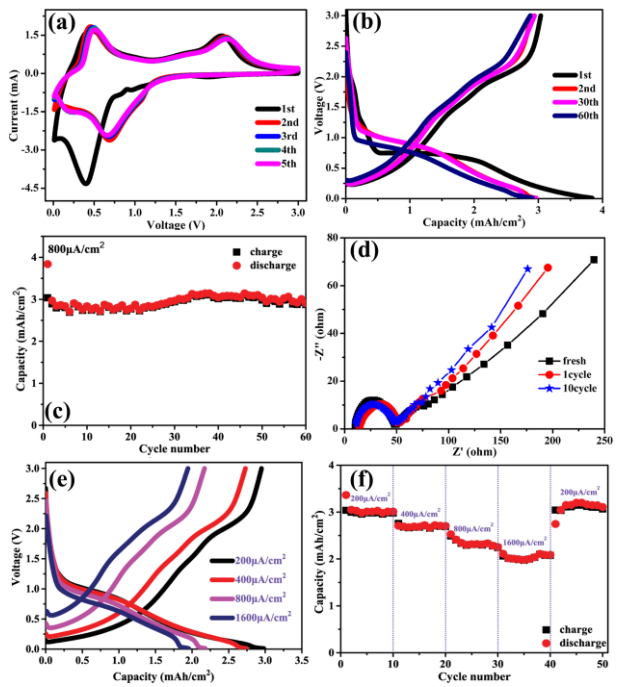

Figure 3 Electrochemical properties of the $MnCo_2O_4$/carbon cloth for lithium storage. (a) The first five consecutive CVs at a scanning rate of 0.5 mV s^{-1}. (b) 1st, 2nd, 30th and 60th charge/discharge curves. (c) Cycling performance at a current density of 800 μA cm^{-2}. (d) The impendance spectra after different cycles of discharge/charge at 200 μA cm^{-2}. (e) The galvanostatic charge/discharge curves at different current densities. (f) Rate performance at different current densities.

The galvanostatic discharge-charge profiles for the 1st, 2nd, 30th and 60th cycles at a current density of 800 μA cm^{-2} are exhibited in Figure 3b. The initial charge and discharge capacity are 3.9 and 3.05 mAh cm^{-2}, corresponding to a coulombic efficiency of 78%. The irreversible capacity loss during the first cycle is likely to be the incomplete decomposition of Li_2O and the difficult dissolution of the SEI, similar to other reported results.[20] The discharge capacity of the representative cycles except for the first cycle are almost around 3.0 mAh cm^{-2}, displaying little capacity loss. Figure 3c is the discharge/charge capacities versus cycle number at a rate of 800 μA cm^{-2}, which clearly reveals that the capacity displays a little decreased, then a little increased and at last stable around 3.0 mAh cm^{-2} even after 60 cycles. In order to get rid of the influence of the carbon cloth, the pure carbon cloth based electrode was also measured, exhibiting a capacity of 0.7 mAh cm^{-2} under same test condition (Figure S2). When coated with electrode material, the carbon cloth has relatively little contact with the electrolyte. Therefore the substrate contributes little to the whole capacity in consistent with the results of Figure 3b, presenting that the main capacity can be ascribed to the voltage plateau. In addition, to the best of our knowledge the high areal capacity obtained from the $MnCo_2O_4$/carbon cloth electrode is much higher than the previous reports about other materials or substrates, such as $MnCo_2O_4$ nanowires arrays on stainless steel foil[17] (0.175 mAh cm^{-2} after 30 cycles at 280 μA cm^{-2}), Fe_3O_4 film (0.414 mAh cm^{-2} after 50 cycles at 10 μA cm^{-2}),[40] SnO_2@Si/carbon cloth[34] (1.35 mAh cm^{-2} after 50 cycles at 380 μA cm^{-2}) and SnO_2@TiO_2/carbon cloth[41] (2.2 mAh cm^{-2} after 50 cycles at 600 μA cm^{-2}). Therefore in our research the high areal capacity of the $MnCo_2O_4$/carbon cloth has been obtained presenting the superior performance in lithium storage properties.

In order to further reveal the transport kinetics, electrochemical impendance spectra were measured after different cycles of discharge and charge at 200μA cm^{-2} (Figure 3d). The plots consist of a depressed semicircle in the high and middle frequency regions and a straight line in the low frequency region. The semicircle at high frequency can be assigned to the SEI film and contact resistance (R_{SEI}), while that at middle frequency is attributed to the charge-transfer impendance on electrode-electrolyte interface (R_{ct}).[42] Small changes of R_{SEI} and R_{ct} have been shown from the plots, implying that the reversible reactivity in the discharge/charge cycles. In addition, from the low frequency inclined line, the lithium-ion diffusion process is easier as with the increasing cycle number, which is likely to be an activated process. Therefore, this fact again confirms the excellent reversible reactivity during the insertion/desertion of lithium-ion in the assembled-nanostructure.

Since the rate capability is also an important parameter for lithium-ion batteries, we also investigate the rate performances of the $MnCo_2O_4$-based electrodes by charging/discharging at different rates ranging from 200-1600 μA cm^{-2}. From Figure 3e-f, it can be seen that the capacity decreases from 3, 2.8, 2.25 to 2 mAh cm^{-2} with increased rate from 200, 400, 800, to 1600 μA cm^{-2}. The capacity is then reversibly back to 3 mAh cm^{-2} once the charge/discharge rate was set back to 200 μA cm^{-2} again. The corresponding ratios of charge/discharge capacity as well as coulombic efficiency are almost approaching 100%, which can be

concluded from the approximate capacity of charge and discharge, presenting the excellent battery performance. Based on the above results, the $MnCo_2O_4$ with mixed valence states of Co and Mn is an excellent anode material.

Since Co_3O_4 has the same crystal structure, approximate lattice constant with $MnCo_2O_4$ and the only difference is the partial substitution of Co with Mn cation, it is quite important to compare the electrochemical properties between Co_3O_4 and $MnCo_2O_4$. Hierarchical Co_3O_4 nanosheets arrays were first grown on carbon cloth via a similar hydrothermal and annealing process. Figure 4a is the XRD pattern of the annealed sample, where all the peaks, except these marked with "★" coming from carbon cloth, can be indexed to pure spinel Co_3O_4 (JCPDS no.42-1467). Figure 4b-c shows the SEM images of the products at different magnifications. Similar to the $MnCo_2O_4$ samples, the Co_3O_4 products are also with nanosheets morphology, which were grown uniformly on the whole carbon microfiber, forming into hierarchical structure. The electrochemical performances of the Co_3O_4/carbon cloth electrodes were also investigated by configuring them as CR2032 coin cells. The galvanostatic discharge-charge profiles for the 1st, 2nd, 30th and 60th cycles at a current density of 800 μA cm^{-2} are exhibited in Figure 4d. The initial charge and discharge capacity are 4.25 and 3.4 mAh cm^{-2} presenting a coulombic efficiency of 80%. The discharge capacity of the representative cycles except for the first cycle are almost around 3.5 mAh cm^{-2} with little capacity loss. Figure 4e is the discharge/charge capacities versus cycle number at a rate of 800 μA cm^{-2}, which clearly reveals that the capacity displays a little increased and then stable around 3.5 mAh cm^{-2} even after 60 cycles. Figure 4f shows that the capacity decreases from 3.5, 3, 2.7, 2.5 to 2 mAh cm^{-2} with increasing the rate from 200, 400, 800, 1600 to 3200 μA cm^{-2}, and the capacity could be reversibly back to 3.5 mAh cm^{-2} once the charge/discharge rate was set back to 200 μA cm^{-2} again. The capacities remain stable almost at every current density.

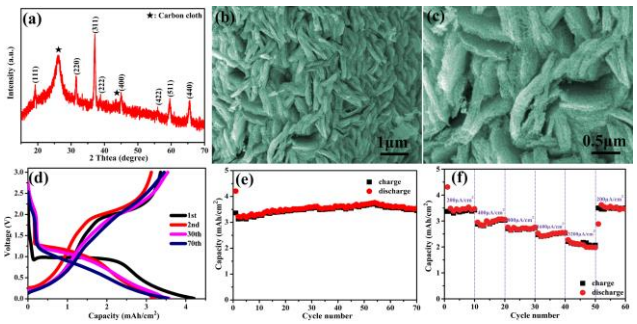

Figure 4 The XRD pattern (a) and SEM images (b,c) at different magnifications of Co_3O_4/carbon cloth. Electrochemical properties of the Co_3O_4 nanosheets for lithium storage: (d) 1st, 2nd, 30th and 60th charge/discharge curves. (e) Cycling performance at a current density of 800 μA cm^{-2}. (f) Rate performance at different current densities.

In order to further investigate the $MnCo_2O_4$ performances, which could be considered as the partial replacement of Co by Mn in Co_3O_4, the first charge/discharge capacity versus voltage profiles are presented in Figure 5a-b. Both of the two products have obvious plateau meaning the main capacity around the plateau voltage. However it is also evident that after the introduction of Mn species the voltage plateau becomes lower whatever the current density of 200 or 800 μA cm^{-2}. In addition at the current density of 800 μA cm^{-2} the voltage plateau dropping can achieve 0.25 V. Meanwhile the capacities of $MnCo_2O_4$ are comparable with the Co_3O_4, displaying just only a little lower. As it is well known that the Mn-based metal oxides perform worse than the Co-based metal oxides due to their bad conductivity. Nonetheless here in our research the performances of $MnCo_2O_4$ are almost well compared to Co_3O_4. Considering the reduced average voltage of $MnCo_2O_4$ leading to increased output voltage of a lithium-ion full cell, the full cells were also assembled with commercial $LiCoO_2$/Al foil as cathode. The cycling performance of the commercial cathode are shown in Figure S3 displaying a capacity of 2.5 mAh cm^{-2} after 80 cycles at a current density of 800 μA cm^{-2}.The capacity versus voltage profiles of the full cells are shown in Figure 5c-d displaying cathode-limited capacities. The results display that the capacities of $MnCo_2O_4$ are obviously higher than the Co_3O_4 likely due to the fact that in the certain voltage window of 1.8-4.0 V the $MnCo_2O_4$ has a little lower average voltage as well as higher output voltage in full cells. The rate performances of the two materials based electrodes again demonstrate the superior property of $MnCo_2O_4$ shown in Figure 5e. The capacities are higher in almost all of the current densities. Besides, it was found that the capacities are slowly decreasing in the first several cycles, the reason may be the wasting of cathode material in full cells before reversible cycling occurring as well as the irreversible reaction in the first several cycles.[43,44] The corresponding coulombic efficiency plots (Figure 5f) are almost around 100% except the first cycle. Evidently owing to the special crystal structure of $MnCo_2O_4$, the performances of full cells are better when compared to Co_3O_4.

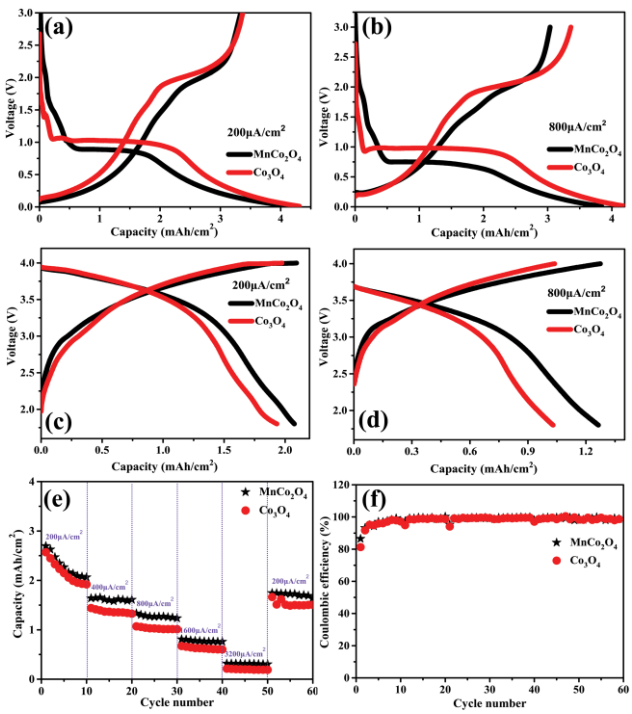

Figure 5 The capacity versus voltage curves of half cells (a,b) and full cells (c,d) at different current densities. The rate performances (e) and coulombic efficiency (f) of the full cells assembled with commercial $LiCoO_2$/Al foil as cathode.

Figure 6a shows the unit cell consisting of O^{2-} (yellow) and

cations of +2 (red) and +3 (blue) whatever $MnCo_2O_4$ or Co_3O_4, presenting the mixed valence oxides that adopt the same spinel structure. Figure 6b clearly displays the detailed structure which can be regarded as the O atoms with cubic closest packing and the cations of +2 and +3 respectively distributed over tetrahedral and octahedral stacking interstices. Therefore the $MnCo_2O_4$ could have the same excellent electrochemical performances with Co_3O_4. In order to further investigate the kinetics of lithium ion insertion/extraction at the electrode/electrolyte interface and rate of lithium diffusion in the film we have performed the CV measurements at different scanning rates. As with the sweep rate increasing the cathodic and anodic peaks move to lower and higher potentials, which can clearly reflects kinetics of lithium insertion/extraction at the electrode/electrolyte interface and rate of lithium diffusion in the film.[45] Figure 6c-d shows the CV curves of the $MnCo_2O_4$ and Co_3O_4 electrodes at scan rates of 0.2-0.8 mV s^{-1} in the voltage range of 0.01-3.0 V after 5th, 10th and 15th cycles. As the scan rates increase, the peaks moved respectively, with the increase of magnitude of peak currents. Furthermore since the loading mass of the two materials are almost the same, the ratio of Co species is about 2/3. Then in the subsequent comparation of peak values we chose the current values as its original 2/3. Then in Figure 6c and 6d, linear correlation was established between the peak currents and the square roots of scan rates for both peak 1 and peak 2 according to the Randles-Sevcik equation:

$$I_p = (2.69\times10^5)n^{3/2}AD^{1/2}\upsilon^{1/2}\Delta C_0$$

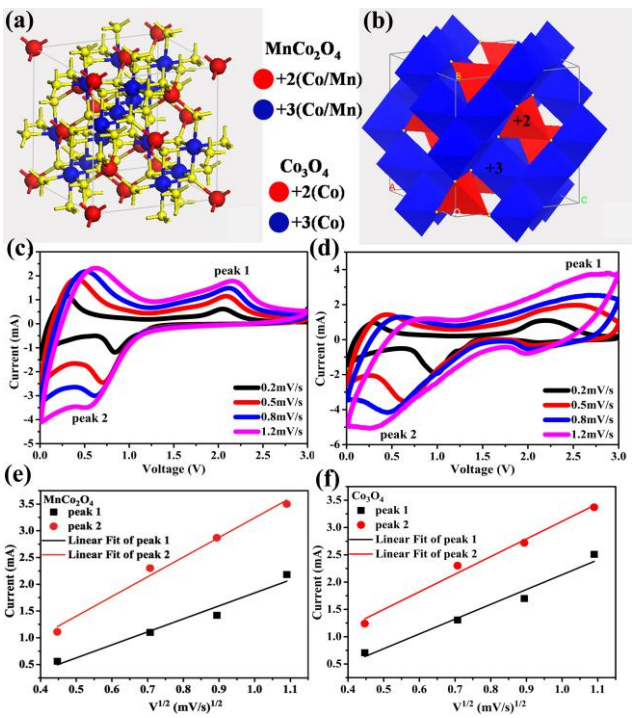

Figure 6 (a,b) Structural illustrations of $MnCo_2O_4$ and Co_3O_4 presenting the same crystal structure and the different Mn and Co position sites. CV curves and peak currents versus square root of scan rates of (c,e) the $MnCo_2O_4$ and (d,f) Co_3O_4 electrodes scanned at 0.2, 0.5 and 0.8mV s^{-1} after 5th, 10th and 15th cycles.

Where I_p is the peak current; n is the number of transfer electrons; A is the surface area of electrodes; D is the diffusion coefficient; υ is the scan rate and ΔC_0 is the concentration of reaction. The slopes for peak 1 and peak 2 on the $MnCo_2O_4$ are almost the same with the Co_3O_4, revealing that even with the introduction of Mn species with poor performances there was little influence on the lithium diffusion coefficient, resulting in excellent electrochemical performance for lithium storage.

Conclusions

In summary, we have developed a facile strategy for the preparation of hierarchical $MnCo_2O_4$ nanosheets arrays/carbon cloth exhibiting high capacity, excellent cycling stability and good rate performances. Using the flexible cloth directly as anode, we fabricated binder-free coin cells with high areal capacity of 3.0 mAh cm^{-2} at a current density of 800 μA cm^{-2}, which is just a little lower than the Co_3O_4/carbon cloth fabricated by the same method. Considering the reduced average voltage as well as increased output voltage of a full cell induced by the introduction of Mn species with a lower lithium extraction potential, the full cells of $MnCo_2O_4$ have been demonstrated relatively higher or comparative capacity with the Co_3O_4 in a potential range of 1.8-4.0 V. The capacity versus voltage curves of both half and full cells have confirmed the lower voltage plateau and superiority performances of $MnCo_2O_4$. In addition the crystal structures have been analyzed exhibiting the little difference of partially replacing Co by Mn. Meanwhile the lithium-ion diffusion has not been affected by the introduction of Mn with poor conductivity demonstrating the excellent electrochemical performances of $MnCo_2O_4$. This facile method of fabricating transition metal oxides may hold promise in the synthesis of multiphasic oxides such as Co or Mn based materials with any ratio and the partial replacement of Co by Mn pave a way for high full cell performances of Co-based oxides.

Acknowledgement

This work was supported by the National Natural Science Foundation (61377033, 91123008) and the Fundamental Research Funds for the Central Universities (HUST: 2013NY013). We thank the Analytical and Testing Center of Huazhong University Science & Technology and the Center of Micro-Fabrication and Characterization (CMFC) of WNLO for the samples measurements.

Notes and references

[a] *Wuhan National Laboratory for Optoelectronics and School of Optical and Electronic Information, Huazhong University of Science and Technology, Wuhan 430074, China. Fax: 86 27 87792225; E-mail: dichen@mail.hust.edu.cn (D.C)*

[b] *State Key Laboratory for Superlattices and Microstructures, Institute of Semiconductors, Chinese Academy of Sciences, Beijing 100083, China gzshen@semi.ac.cn (G.S)*

†Electronic Supplementary Information (ESI) available: [The XRD pattern of the $MnCo_2O_4$ powders, the cycling performance of the pure carbon cloth based electrode at a current density of 800 μA cm^{-2}, the cycling performance of the commercial $LiCoO_2$/Al foil based electrode at a current density of 800 μA cm^{-2}.]. See DOI: 10.1039/b000000x/

1 G. M. Zhou, F. Li and H. M. Cheng, *Energy Environ. Sci.*, 2013, DOI: 10.1039/C3EE43182G.

2 S.Y. Lee, K. H. Choi, W. S. Choi, Y. H. Kwon, H. R. Jung, H. C. Shin and J. Y. Kim, *Energy Environ. Sci.*, 2013, **6**, 2414-2423.

3 P. G. Bruce, B. Scrosati and J. M. Tarascon, *Angew. Chem. Int. Ed.*, 2008, **47**, 2930-2946.

4 B. Liu, P. Soares, C. Checkles, Y. Zhao and G. H. Yu, *Nano Lett.*, 2013, **13**, 3414-3419.

5 Y. H. Lee, J. S. Kim, J. Noh, I. Lee, H. J. Kim, S. Choi, J. Seo, S. Jeon, T. S. Kim, J. Y. Lee and J. W. Choi, *Nano Lett.*, 2013, **13**, 5753-5761.

6 J. Y. Choi, D. J. Lee, Y. M. Lee, Y. G. Lee, K. M. Kim, J. K. Park and K. Y. Cho, *Adv. Funct. Mater.*, 2013, **23**, 2108-2114.

7 X. F. Wang, Q. Y. Xiang, B. Liu, L. J. Wang, T. Luo, D. Chen and G. Z. Shen, *Sci. Rep.*, 2013, **3**, 2007.

8 B. Liu, J. Zhang, X. F. Wang, G. Chen, D. Chen, C. W. Zhou and G. Z Shen, *Nano Lett.*, 2012, **12**, 3005-3011.

9 Y. M. Sun, X. L. Hu, W. Luo, F. F. Xia and Y. H. Huang, *Adv. Funct. Mater.*, 2013, **23**, 2436-2444.

10 D. Q. Liu, X. Wang, X. B. Wang, W. Tian, Y. Bando and D. Golberg, *Sci. Rep.*, 2013, **3**, 2543.

11 L. M. Wang, B. Liu, S. H. Ran, H. T. Huang, X. F. Wang, B. Liang, D. Chen and G. Z. Shen, *J. Mater. Chem.*, 2012, **22**, 23541-23546.

12 H. Huang, W. J. Zhu, X. Y. Tao, Y. Xia, Z. Y. Yu, J. W. Fang, Y. P. Gan and W. K. Zhang, *ACS Appl. Mater. Interfaces*, 2012, **4**, 5974-5980.

13 Y. Q. Fan, H. B. Shao, J. M. Wang, L. Liu, J. Q. Zhang and C. N. Cao, *Chem. Commun.*, 2011, **47**, 3469-3471.

14. L. Chang, L. Q. Mai, X. Xu, Q. Y. An, Y. L. Zhao, D. D. Wang and X. Feng, *RSC Adv.*, 2013, **3**, 1947-1952.

15. Y. C. Qiu, G. L. Xu, K. Y. Yan, H. Sun, J. W. Xiao, S. H. Yang, S. G. Sun, L. M. Jin and H. Deng , *J. Mater. Chem.*, 2011, **21**, 6346-6353.

16 H. L. Wang, L. F. Cui, Y. Yang, H. S. Casalongue, J. T. Robinson, Y. Y. Liang, Y. Cui and H. J. Dai, *J. AM. CHEM. SOC.*, 2010, **132**, 13978-13980.

17 L. Yu, L. Zhang, H. B. Wu, G. Q. Zhang and X. W. Lou, *Energy Environ. Sci.*, 2013, **6**, 2664-2671.

18 H. B. Wu, H. Pang and X. W. Lou, *Energy Environ. Sci.*, 2013, **6**, 3619-3626.

19 L. J. Wang, B. Liu, S. H. Ran, L. M. Wang, L. N. Gao, F. Y. Qu, D. Chen and G. Z. Shen, *J. Mater. Chem. A*, 2013, **1**, 2139-2143.

20 J. F. Li, S. L. Xiong, X. W. Lia and Y. T. Qian, *Nanoscale*, 2013, **5**, 2045-2054.

21 L. Hu, H. Zhong, X. R. Zheng, Y. M. Huang, P. Zhang and Q. W. Chen, *Sci. Rep.*, 2012, **2**, 986.

22 H. L. Wang, Y. Yang, Y. Y. Liang, G. Y. Zheng, Y. G. Li, Y. Cui and H. J. Dai, *Energy Environ. Sci.*, 2012, **5**, 7931-7935.

23 J. F. Li, S. L. Xiong, X. W. Li and Y. T. Qian, *J. Mater. Chem.*, 2012, **22**, 23254-23259.

24 Z. Y. Wang, Z. C. Wang, W. T. Liu, W. Xiao and X. W. Lou. *Energy Environ. Sci.*, 2013, **6**, 87-91.

25 P. Lavela, J. L. Tirado and C. Vidal-Abarca, *Electrochimica Acta*, 2007, **52**, 7986-7995.

26 J. F. Li, J. Z. Wang, X. Liang, Z. J. Zhang, H. K. Liu, Y. T. Qian and S. L. Xiong, *ACS Appl. Mater. Interfaces*, 2014, **6**, 24-30.

27 L. Li, Y. Q. Zhang, X. Y. Liu, S. J. Shi, X.Y. Zhao, H. Zhang, X. Ge, G. F. Cai, C. D. Gu, X. L. Wang and J. P. Tu, *Electrochimica Acta*, 2014, **116**, 467-474.

28 S. G. Mohamed, T. F. Hung, C. J. Chen, C. K. Chen, S. F. Hu and R. S. Liu, *RSC Adv.*, 2014, **4**, 17230-17235.

29 C. C Fu, G. S Li, D. Luo, X. S. Huang, J. Zheng and L. P. Li, *ACS Appl. Mater. Interfaces*, 2014, **6**, 2439-2449.

30 T. Y. Ma, Y. Zheng, S. Dai, M. Jaroniecb and S. Z. Qiao, *J. Mater. Chem. A*, 2014, DOI: 10.1039/c4ta01672f.

31 Y. X. Tang, X. H. Rui, Y. Y. Zhang, T. M. Lim, Z. L. Dong, H. H. Hng, X. D. Chen, Q. Y. Yan and Z. Chen, *J. Mater. Chem. A*, 2013, **1**, 82-88.

32 Y. Y. Zhang, Y. X. Tang, S. Y. Yin, Z. Y. Zeng, H. Zhang, C. M. Li, Z. L. Dong, Z. Chen and X. D. Chen, *Nanoscale*, 2011, **3**, 4074-4077.

33 S. Y. Yin, Y. Y. Zhang, J. H. Kong, C. J. Zou, C. M. Li, X. H. Lu, J. Ma, F. Y. C. Boey and X. D. Chen, *ACS Nano*, 2011, **5**, 3831-3838.

34 W. N. Ren, C. Wang, L. F. Lu, D. D. Li, C. W. Cheng, J. P. Liu, *J. Mater. Chem. A*, 2013, **1**, 13433-13438.

35 Z. R. Wang, H. Wang, B. Liu, W. Z. Qiu, J. Zhang, S. H. Ran, H. T. Huang, J. Xu, H. W. Han, D. Chen and G. Z. Shen, *ACS Nano*, 2011, **5**, 8412-8419.

36 Y. S. Luo, J. S. Luo, J. Jiang, W. W. Zhou, H. P. Yang, X. Y. Qi, H. Zhang, H. J. Fan, D. Y. W. Yu, C. M. Li and T. Yu, *Energy Environ. Sci.*, 2012, **5**, 6559-6566.

37 X. J. Hou, B. Liu, X. F. Wang, Z. R. Wang, Q. F. Wang, D. Chen and G. Z. Shen, *Nanoscale*, 2013, **5**, 7831-7837.

38 L. Zhou, D. Y. Zhao and X. W. Lou, Adv. Mater., 2012, **24**, 745-748.

39 G. N. Zhu, Y. G. Wang and Y. Y. Xia, *Energy Environ. Sci.*, 2012, **5**, 6652-6667.

40 S. Mitra, P. Poizot, A. Finke and J. M. Tarascon, *Adv. Funct. Mater.*, 2006, **16**, 2281-2287.

41 X. J. Hou, X. F. Wang, B. Liu, Q. F. Wang, Z. R. Wang, D. Chen and G. Z. Shen, *ChemElectroChem*, 2014, **1**, 108-115.

42 Y. Z. Su, S. Li, D. Q. Wu, F. Zhang, H. W. Liang, P. F. Gao, C. Cheng and X. L. Feng, *ACS Nano*, 2012, **6**, 8349-8356.

43 J. Hassoun, K. S. Lee, Y. K. Sun and B. Scrosati, *J. Am. Chem. Soc.*, 2011, **133**, 3139-3143.

44 M. C. López, G. F. Ortiz, P. Lavela, R. Alcántara and J. L. Tirado, *ACS Sustainable Chem. Eng.*, 2013, **1**, 46-56.

45 A. Rougier, K. A. Striebel, S. J. Wen and E. i. Cairns, *J. Electrochem. Soc.*, 1998, **145**, 2975-2980.